





Article

Phellinus baumii Polyphenol: A Potential Therapeutic Candidate against Lung Cancer Cells

Xue Liu ^{1,†} , Shiyao Cui ^{1,2,†}, Caiyun Dan ¹, Wenle Li ¹, Hongqing Xie ¹, Conghui Li ¹ and Liangen Shi ^{1,*} 

¹ College of Animal Sciences, Zijingang Campus, Zhejiang University, Hangzhou 310058, China

² College of Life Sciences, Yungu Campus, Westlake University, Hangzhou 310058, China

* Correspondence: slgsilk@zju.edu.cn; Tel.: +86-13-0189-47056 or +86-15-3558-15905

† These authors contributed equally to this work.

Abstract: *Phellinus baumii*, a fungus that grows on mulberry trees and is used in traditional Chinese medicine, exerts therapeutic effects against various diseases, including cancer. Polyphenols, generally considered to be antioxidants, have antitumor and proapoptotic effects. In this study, we identified the composition of *Phellinus baumii* polyphenol (PBP) and characterized its 17 chemical components by UPLC–ESI–QTOF–MS. Furthermore, to clarify the potential mechanism of PBP against Lung Cancer Cells, network pharmacology and experimental verification were combined. Molecular docking elucidated the binding conformation and mechanism of the primary active components (Osmundacetone and hispidin) to the core targets CASP3, PARP1 and TP53. In addition, potential molecular mechanisms of PBP predicted by network pharmacology analysis were validated in vitro. PBP significantly inhibited the human lung cancer A549 cells and showed typical apoptotic characteristics, without significant cytotoxicity to normal human embryonic kidney (HEK293) cells. Analysis using flow cytometry and western blot indicated that PBP caused apoptosis, cell cycle arrest, reactive oxygen species (ROS) accumulation, and mitochondrial membrane potential (MMP) depression in A549 cells to exercise its antitumor effects. These results reveal that PBP has great potential for use as an active ingredient for antitumor therapy.

Keywords: antitumor activity; caspase-dependent intrinsic mitochondria apoptosis; cell cycle arrest; network pharmacology; *Phellinus baumii* polyphenols; UPLC–ESI–QTOF–MS



Citation: Liu, X.; Cui, S.; Dan, C.; Li, W.; Xie, H.; Li, C.; Shi, L. *Phellinus baumii* Polyphenol: A Potential Therapeutic Candidate against Lung Cancer Cells. *Int. J. Mol. Sci.* **2022**, *23*, 16141. <https://doi.org/10.3390/ijms232416141>

Academic Editor: Alain Chapel

Received: 28 November 2022

Accepted: 13 December 2022

Published: 17 December 2022

Publisher's Note: MDPI stays neutral with regard to jurisdictional claims in published maps and institutional affiliations.



Copyright: © 2022 by the authors. Licensee MDPI, Basel, Switzerland. This article is an open access article distributed under the terms and conditions of the Creative Commons Attribution (CC BY) license (<https://creativecommons.org/licenses/by/4.0/>).

1. Introduction

Cancer significantly affects public health globally [1]. However, the efficiency of many traditional tumor treatments, such as surgery, radiotherapy and chemotherapy, is not ideal due to their severe side effects. Thus, new therapeutic approaches are urgently needed. In recent years, natural products, as a valuable source of antitumor compounds, have gained increasing attention due to their few adverse effects. Many studies have suggested that polyphenols, which are generally recognized as antioxidants, possess antitumor and proapoptotic effects [2,3]. Polyphenols from the pinecones of *Pinus koraiensis* significantly inhibited S180 cell growth by activating the mitochondrial apoptotic pathway [4]. It has been demonstrated that polyphenols from green tea have prophylactic and therapeutic effects against tumors [5]. Resveratrol, a nonflavonoid polyphenol present in grapes, soybeans, peanuts, etc., displays therapeutic potential in breast cancer treatment [6]. Resveratrol can also inhibit murine hepatocellular carcinoma by downregulating CD 8+, CD 122+, Tregs cells [7]. However, the antitumor efficiency of polyphenols remains to be explored and utilized.

Phellinus baumii (*P. baumii*) is a well-known medicinal fungus belonging to *Phellinus*, *Hymenochaetaeaceae*, *Aphylllophorales*, *Hymenomyces*, and *Basidiomycotas*. In China, the fruiting bodies of *P. baumii* have been used as a traditional medicine for centuries [8]. *Phellinus* spp. show a wide range of pharmacological activities, especially anticancer properties, and have

the reputation of ‘forest gold’ due to their abundant components, including polysaccharides, polyphenols, terpenoids, steroids, etc. The polysaccharide extract of *P. baumii* showed toxicity to tumor cells in vitro [9,10] and was found to alleviate ulcerative colitis [11] and high-fat high-fructose diet-induced insulin resistance in mice [12]. The terpenoids produced by *Phellinus* spp. were found to enhance immune function [13,14]. The ethanol extract of *P. baumii* exerted cytotoxic activity against many kinds of human tumor cell lines [15]. Polyphenols of *Phellinus* spp. have been found to have anti-inflammatory and antidiabetic effects on diabetic mice [16,17]. However, whether *P. baumii* polyphenols have antitumor effects is unclear.

In recent years, network pharmacology has become one of the frontiers and hotspots in the field of traditional Chinese medicine research [18]. Network pharmacology research is based on high-throughput omics data analysis, computer virtual computing and network database retrieval. It is a good bioinformatics method to reveal the therapeutic effect of natural drugs with complex components on diseases.

In this study, we identified the components of polyphenol extract from *Phellinus baumii* (PBP) by UPLC–ESI–QTOF–MS for the first time. Additionally, we integrated network pharmacology with experimental verification to clarify the possible mechanism of against lung cancer cells effect of PBP.

2. Results

2.1. Characterization of the Chemical Constituents of PBP

The identification of the components of PBP was performed using UPLC–ESI–QTOF–MS. The base peak chromatograms of PBP in negative ion mode are shown in Figure 1a. A total of 17 peaks were tentatively identified (Table 1). Four peaks (peak 1, 2, 5 and 7) were confirmed qualitatively with a mixed standard of protocatechuic aldehyde (PubChem CID: 8768), caffeic acid (PubChem CID: 689043), osmundacetone (PubChem CID: 9942292) and hispidin (PubChem CID: 54685921) (Figure 1b). Eight compounds were previously reported to exist in the *P. baumii*, including phellibaumin B (peak 4, PubChem CID: 53248680) [19], hypholomine B (peak 6, PubChem CID: 54730031) [20,21], interfungin B (peak 8, PubChem CID: 54718836) [19,22], phelligridimer A (peak 10, PubChem CID: 16155688) [19,23], davallialactone (peak 12, PubChem CID: 54715402) [20,24], phellibaumin E (peak 14, PubChem CID: 54738502) [19,25], phelligridin I (peak 16, PubChem CID: 54689623) [26,27], and inoscavin A (peak 17, PubChem CID: 10434469) [20,24]. Then, five compounds were tentatively identified according to the UPLC–MS results, including kielcorin (peak 3, PubChem CID: 13834128) [28], sterubin (peak 9, PubChem CID: 4872981) [29], (E)-4-(4-hydroxyphenyl)-3-buten-2-one (peak, PubChem CID: 11796857) [30], citrinin (peak 13, PubChem CID: 54680783) [31] and 3-(4,6-Dihydroxy-2-oxochromen-3-yl)-8-hydroxy-2-methoxy-2,3-dihydrofuro [3,2-c] chromen-4-one (peak 15, PubChem CID: 87782626) [32] (Table S1). There were two unknown peaks on the chromatogram with retention times of 9.53 and 11.53 min. The formula of peak N1 is C₁₀H₁₀O₅, and peak N2 was determined to be an isomer of hypholomine B. The 2D chemical structures of PBP compounds are shown in Table 1.

2.2. Identification of Potential Targets of PBP in Lung Cancer Treatment

In total, 221 potential targets of PBP components were collected from the DrugBank and Traditional Chinese medicine systems pharmacology database and analysis platform (TCMSP) databases with 17 components of PBP as keywords (Table S2). A total of 1035 potential lung cancer targets were identified from the OMIM, GeneCards, DisGeNET, and Treatment targets database (TTD) databases (Figure 2a). The intersection of PBP component targets and lung cancer related targets resulted in 60 common targets, which were used as potential targets for subsequent research (Figure 2b and Table S3).

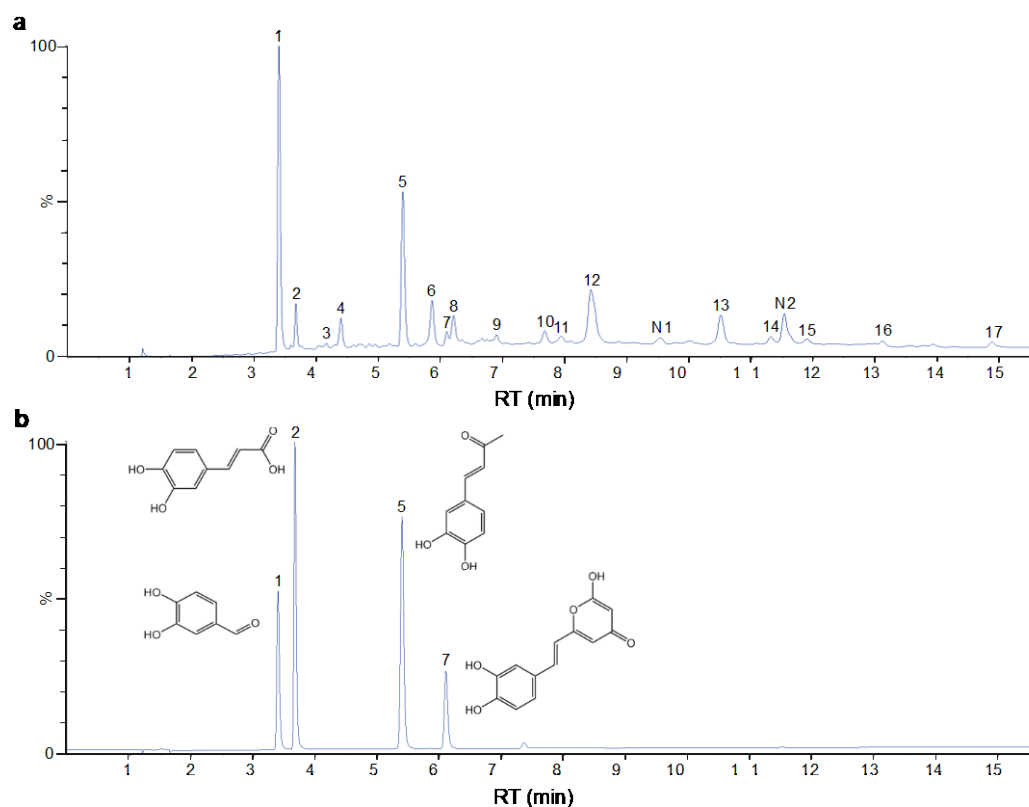


Figure 1. (a) UV chromatogram of PBP at 254 nm. (b) UV chromatogram of mixed standards of protocatechuic aldehyde, caffeic acid, osmundacetone and hispidin.

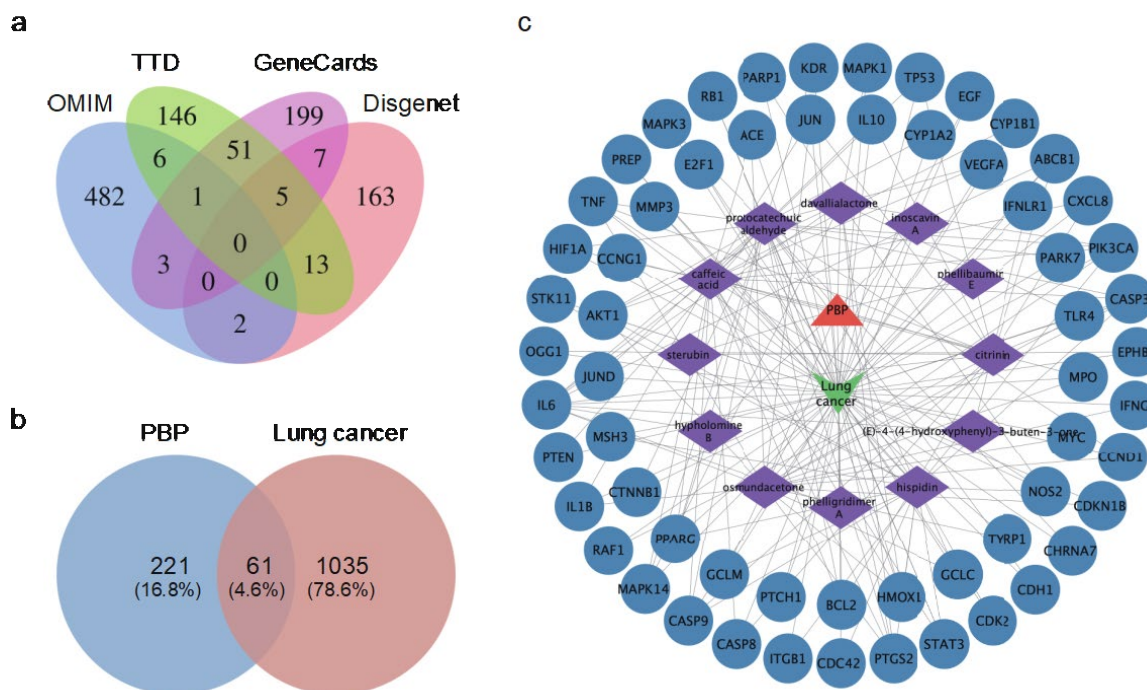
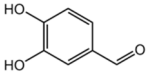
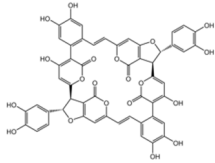
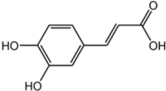
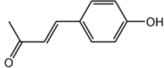
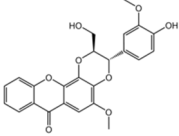
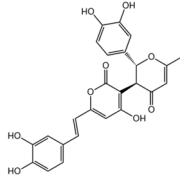
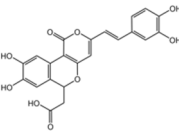
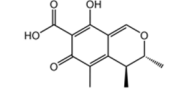
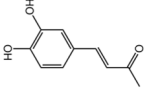
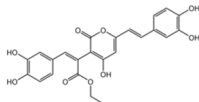
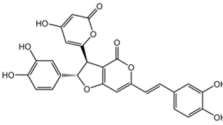
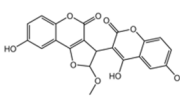
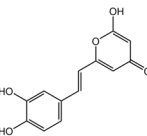
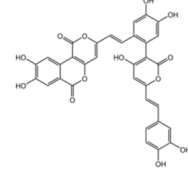
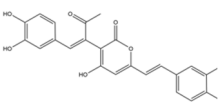
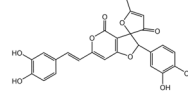


Figure 2. The targets of PBP treat lung cancer and the Components-Disease-Targets network. (a) Venn diagram of lung cancer targets; (b) Venn diagram of PBP treat lung cancer; (c) Drug-Components-Disease-Targets network. The orange triangle represents PBP. The green wedge represents lung cancer. The active substances in PBP are represented by the purple prisms. The targets are shown as blue circles.

Table 1. Characterization of the chemical constituents of PBP by UPLC–ESI–QTOF–MS.

| Peak No. | Formula | Identification | 2D Structure | Peak No. | Formula | Identification | 2D Structure |
|----------|---|-------------------------|---|----------|---|---|---|
| 1 | C ₇ H ₆ O ₃ | protocatechuic aldehyde |  | 10 | C ₅₂ H ₃₂ O ₂₀ | phelligrindimer A |  |
| 2 | C ₉ H ₈ O ₄ | caffeic acid |  | 11 | C ₁₀ H ₁₀ O ₂ | (E)-4-(4-hydroxyphenyl)-3-buten-2-one |  |
| 3 | C ₂₄ H ₂₀ O ₈ | kielcorin |  | 12 | C ₂₅ H ₂₀ O ₉ | davallialactone |  |
| 4 | C ₂₂ H ₁₆ O ₉ | phellibaumin B |  | 13 | C ₁₃ H ₁₄ O ₅ | citrinin |  |
| 5 | C ₁₀ H ₁₀ O ₃ | osmundacetone |  | 14 | C ₂₄ H ₂₀ O ₉ | phellibaumin E |  |
| 6 | C ₂₆ H ₁₈ O ₁₀ | hypholomine B |  | 15 | C ₂₁ H ₁₄ O ₉ | 3-(4,6-Dihydroxy-2-oxochromen-3-yl)-8-hydroxy-2-methoxy-2,3-dihydrofuro [3,2-c] chromen-4-one |  |
| 7 | C ₁₃ H ₁₀ O ₅ | hispidin |  | 16 | C ₃₃ H ₂₀ O ₁₃ | phelligridin I |  |
| 8 | C ₂₃ H ₁₈ O ₈ | interfungin B |  | 17 | C ₂₅ H ₁₈ O ₉ | inoscavin A |  |

2.3. Components-Disease-Targets Interaction Network

To clearly understand the key components of PBP in the treatment of lung cancer, the active Components-Disease-Targets network was visualized using Cytoscape 3.9.1 (Figure 2c). The network contains 74 nodes and 193 edges. The degree value was obtained by CytoNCA tool and ranked in descending order. According to network analysis, compounds have an average degree of 11.0, excluding 5 components with a degree value of 0. The active components greater than the average are shown in Table 2: protocatechuic aldehyde (degree = 26), caffeic acid (degree = 25), osmundacetone (degree = 22), hispidin (degree = 20), citrinin (degree = 15), davallialactone (degree = 11). Therefore, the 6 compounds are considered to be potential bioactive compounds of PBP against lung cancer.

Table 2. Degree of active components and binding energy of docking with CASP3, PARP, TP53.

| Component | Degree | Binding Energy (CASP3) | Binding Energy (PARP) | Binding Energy (TP53) |
|-------------------------|--------|------------------------|-----------------------|-----------------------|
| protocatechuic aldehyde | 26 | - ¹ | - | - |
| caffeic acid | 25 | - | - | - |
| osmundacetone | 22 | −6.4 kcal/mol | −7.2 kcal/mol | −5.3 kcal/mol |
| hispidin | 20 | −6.8 kcal/mol | −7.1 kcal/mol | −6.2 kcal/mol |
| citrinin | 15 | −6.3 kcal/mol | −6.4 kcal/mol | −6.4 kcal/mol |
| davallialactone | 11 | −8.4 kcal/mol | −9.4 kcal/mol | −7.1 kcal/mol |

¹ Molecular docking between the two failed.

2.4. Gene Ontology (GO) and Kyoto Encyclopedia of Genes and Genomes (KEGG) Enrichment Analysis

A total of 312 GO terms with $p < 0.05$, including 214 BP, 43 CC, and 55 MF, were considerably enriched (Table S4). Visual representations of the top 10 considerably enriched terms in the BP, CC, and MF categories were shown (Figure 3a). Furthermore, a total of 150 pathways with $p < 0.05$ were identified (Table S5). The top 20 pathways were displayed in (Figure 3b). The 33 intersection targets were related to ‘pathway in cancer’. Combined with ‘pathway in cancer’ (Figure S1), it can be shown that these potential targets in the ‘pathway in cancer’ are mainly focused on apoptosis and cell cycle-related pathways. The results show that PBP may treat lung cancer by regulating apoptosis and cell cycle progression.

2.5. Protein-Protein Interaction (PPI) Network and Core Targets

A PPI network comprising 60 intersectional targets was created using the STRING database (interaction score > 0.9) to further examine the potential mechanism by which PBP treats lung cancer (Figure 4a). Then the protein interaction results of STRING analysis were visualized by Cytoscape 3.9.1 (Figure 4b). This PPI network is ranked by degree score. Stronger protein interaction was indicated by a higher score. The 6 core targets were obtained: TP53, STAT3, PARP1, HMOX1, AKT1, CASP3. Among them, TP53, PARP1, CASP3 targets are key genes in the pathway in cancer, and are associated with apoptosis and cell cycle progression. PBP may treat lung cancer by acting on these core targets.

2.6. Molecular Docking

Autodock Vina was used to verify the bindings of TP53, PARP1, and CASP3 to the six key active compounds of PBP. The binding energies indicates the degree of complementarity between the components and the targets. The lower the binding energy, the higher the stability. The molecular dockings of Rotocatechuic aldehyde, caffeic acid with TP53, PARP1, CASP3 were failed. The binding energies of osmundacetone with CASP3, PARP and TP53 quercetin and wogonin were −6.4, −7.2, −5.3 kcal/mol, respectively. The binding energies of hispidin with CASP3, PARP and TP53 were −6.8, −7.1, −6.2 kcal/mol, respectively (Table 2). The results of degree and binding energy showed that osmundacetone and hispidin were the main active compounds of PBP treats lung cancer. Next, the molecular docking results of autodock vina were treated with PyMol. As shown in Figure 4c, osmundacetone forms 4 hydrogen bonds with TYR-276, MET-39 and TYR-37 in CASP3, hispidin formed 2 hydrogen bonds with MET-39 and TYR-37 in CASP3. In addition, osmundacetone forms 5 hydrogen bonds with GLY-888, GLU-988, GLY-863, SER-904 and TRP-861 in PARP, hispidin formed 3 hydrogen bonds with GLN-853 and GLU-840 in PARP, osmundacetone forms 1 hydrogen bonds with LEU-330 in TP53, hispidin formed 7 hydrogen bonds with ARG-335, GLY-334, ILE-332, leu-330, THR-329 in TP53 (Figure 4c).

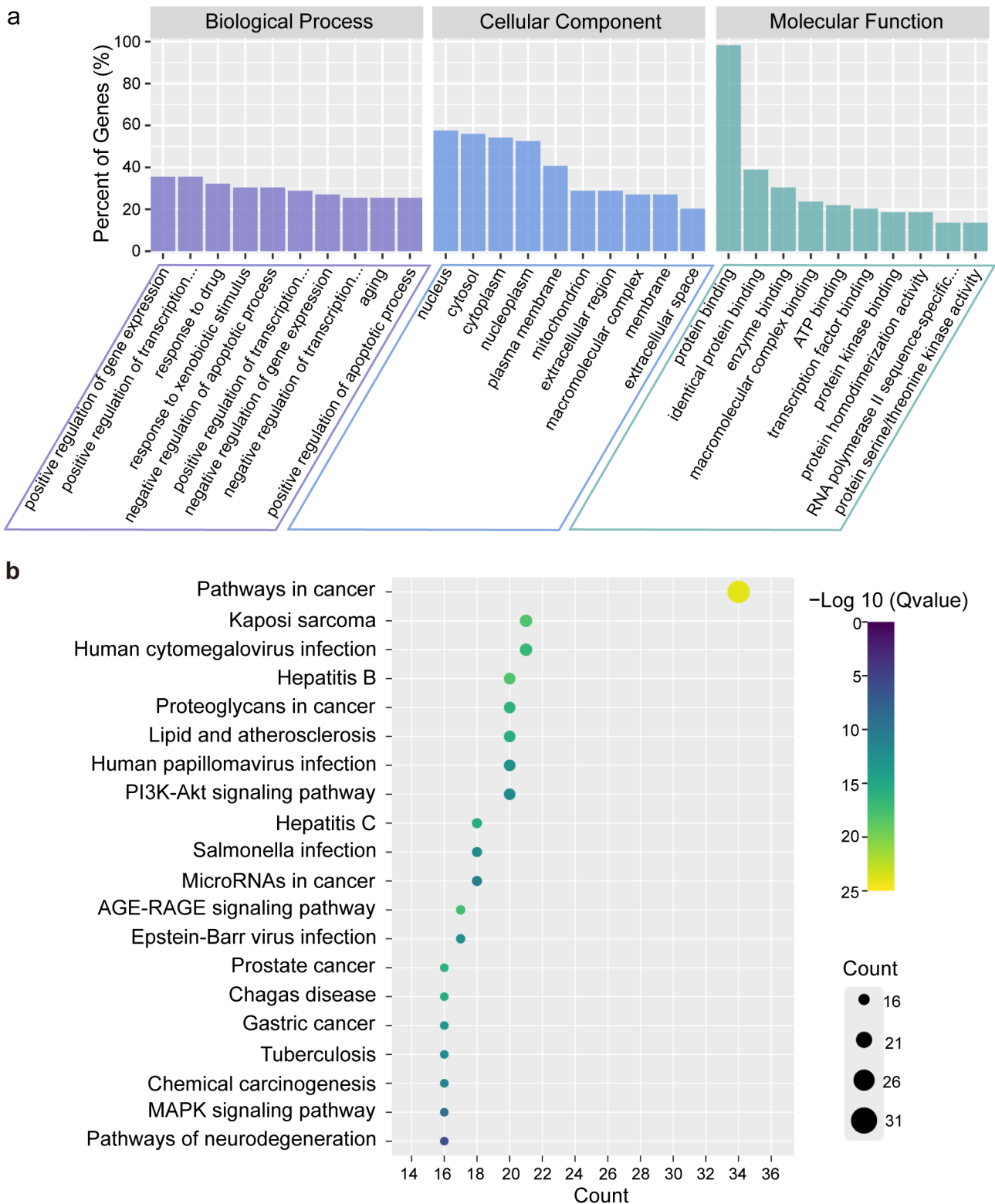


Figure 3. Analysis of GO and KEGG enrichment to identify the anti-tumor mechanisms. (a) The top 10 in BP terms, CC terms, and MF terms of the GO terms ($p < 0.05$); (b) The top 20 KEGG pathways ($p < 0.05$).

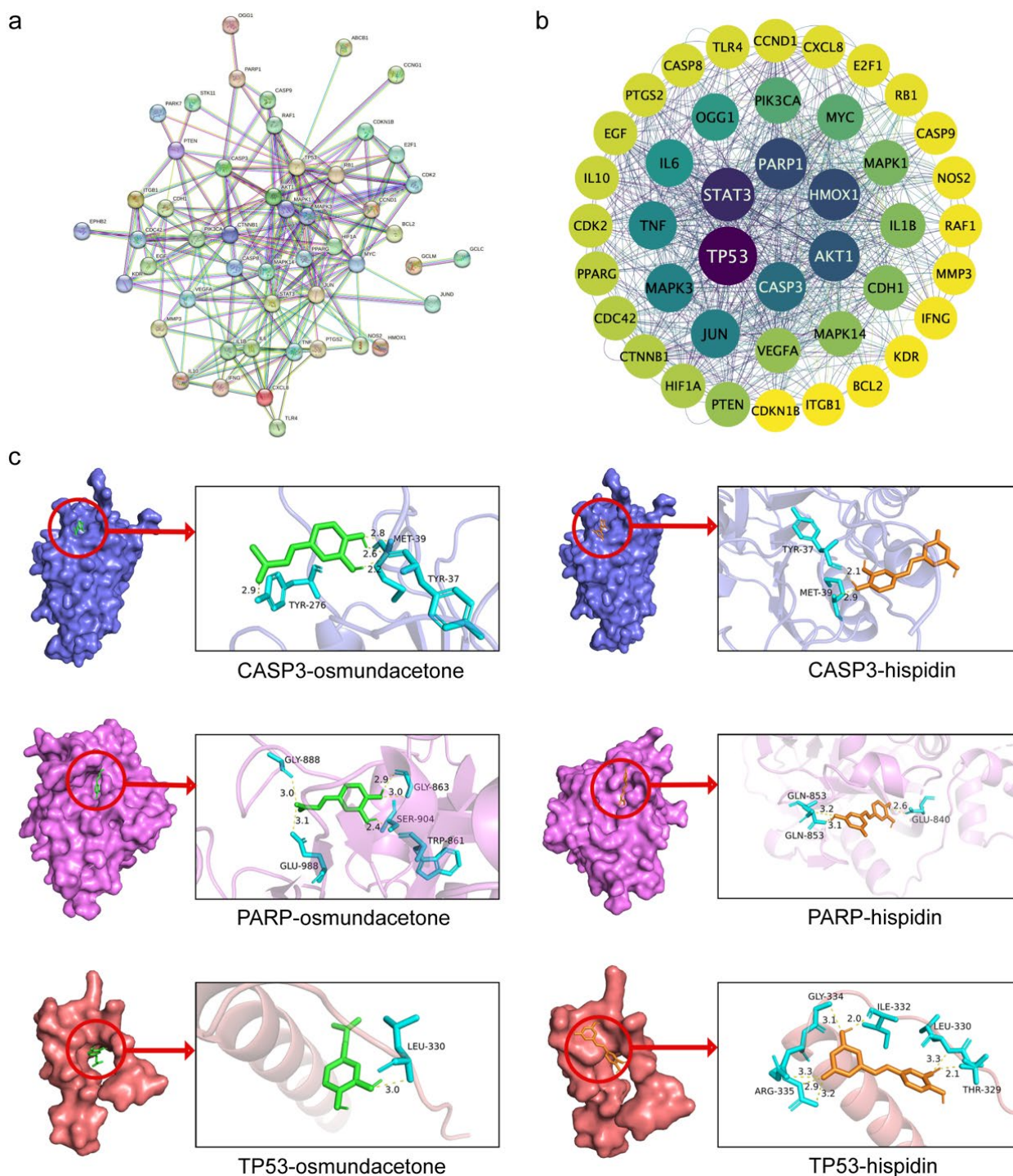


Figure 4. Identification and molecular docking verification of PBP anti-lung cancer core targets. (a) PPI network diagram obtained by STRING database analysis (interaction score > 0.9); (b) Visualizing the PPI network was completed using Cytoscape 3.9.1; (c) The docking mode of CASP3-osmundacetone, PARP-osmundacetone, TP53-osmundacetone, CASP3-hispidin, PARP-hispidin and TP53-hispidin.

2.7. PBP Significantly Inhibited the Viability of A549 Cells

The toxicity of PBP to human tumor cells and normal cells was examined using CCK-8 assays. According to the results, the IC_{50} values against A549 were $49.07 \pm 0.5 \mu\text{g/mL}$ and varied by dose and duration (Figure 5a). In addition, we examined the toxicity of PBP to various human tumor cells. After 48 h treatment of PBP, the IC_{50} values against Hela, HepG2,

T24 and HCT116 cells were 96.14 ± 4.9 , 140.1 ± 9.6 , 105.0 ± 10.7 and 54.05 ± 0.7 $\mu\text{g}/\text{mL}$, respectively (Table 3, Figure A1). However, at doses below 80 $\mu\text{g}/\text{mL}$, PBP had no discernible toxic effects on HEK293 cells (normal cells, not tumor cells) (Figure 5b). These results indicate that PBP is significantly toxic to human lung cancer A549 cells, but not to normal human HEK293 cells.

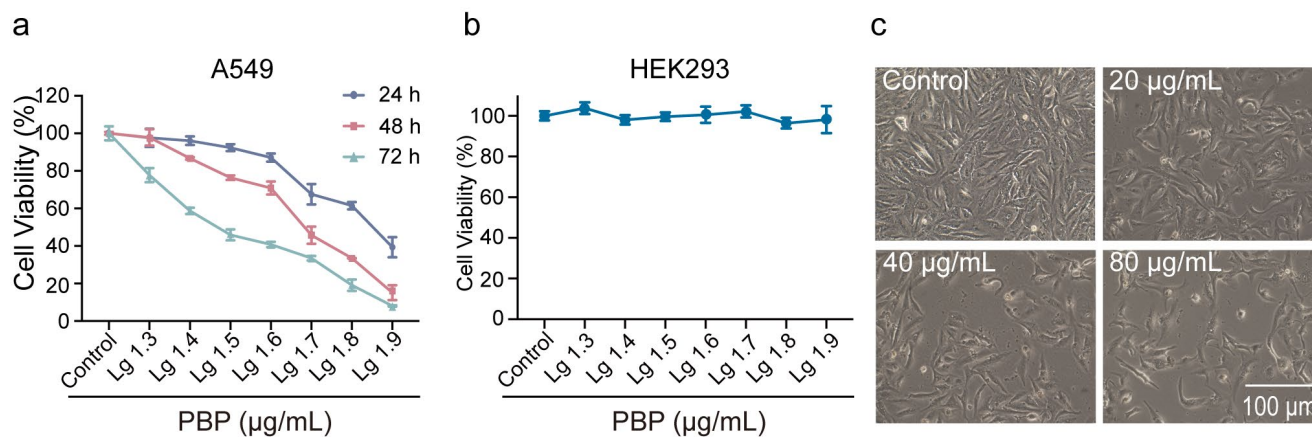


Figure 5. Cytotoxicity of PBP to A549 cells. (a) A549 cells viability was assayed using the CCK-8 assay, after being exposed to varying amounts of PBP for 24, 48, and 72 h; (b) Cytotoxicity of PBP to HEK293 cell in 48 h determined by CCK-8 assays; (c) Typical morphological changes in A549 cells after treatment with PBP for 48 h.

Table 3. Inhibitory effects of PBP on viability of various tumor cells.

| Tumor Cell Lines | A549 | HepG2 | T24 | Hela | HCT116 |
|--|----------------|-----------------|------------------|----------------|----------------|
| IC ₅₀ ($\mu\text{g}/\text{mL}$) | 49.1 ± 0.5 | 140.1 ± 9.6 | 105.0 ± 10.7 | 96.1 ± 4.9 | 54.2 ± 0.7 |

Cell morphology was examined using phase-contrast microscopy to further evaluate the effects of PBP on A549 cells. The A549 cells in the control group were polygonal or fusiform and adhered to the plate well. The A549 cells treated with PBP, however, displayed morphological features such as shrinkage and rounding (Figure 5b). The number of A549 cells dramatically decreased as PBP concentration rose. Under treatment with 80 $\mu\text{g}/\text{mL}$ PBP, the shape of the A549 cells became irregular, and floating cells were clearly observed, forming a smooth contour and separating from the surroundings. Consequently, PBP may induce cell death through certain pathways and impair cell proliferation, which needs to be further confirmed.

2.8. PBP Induced Apoptosis in A549 Cells

Flow cytometry was used to identify cell apoptosis using Annexin V-FITC and PI staining methods. Annexin V⁻/PI⁺ (upper left quadrant) represents cell debris or other causes of cell death cells. Annexin V⁻/PI⁻ (lower left quadrant) represents normal living cells. Annexin V⁺/PI⁺ (upper right quadrant) represents late apoptotic cells. Annexin V⁺/PI⁻ (lower right quadrant) represents early apoptotic cells. The results showed a rise in the total apoptotic rate of A549 cells from $5.20\% \pm 1.5\%$ to $9.72\% \pm 0.28\%$, $18.46\% \pm 1.93\%$ and $25.42\% \pm 0.86\%$, respectively. Notably, the early apoptotic rate increased from $1.3\% \pm 0.56\%$ to $7.37\% \pm 0.87\%$, $18.80\% \pm 2.33\%$ and $32.88\% \pm 1.64\%$, and the late apoptotic rate increased from $3.47\% \pm 0.71\%$ to $6.56\% \pm 0.67\%$, $6.72\% \pm 0.83\%$ and $8.26\% \pm 1.54\%$, respectively (Figure 6a,c). Annexin V⁺ in Figure 6b also confirmed the result that PBP induced A549 cell apoptosis. The results suggested that PBP may influence A549 cell viability by inducing apoptosis in a dosage manner.

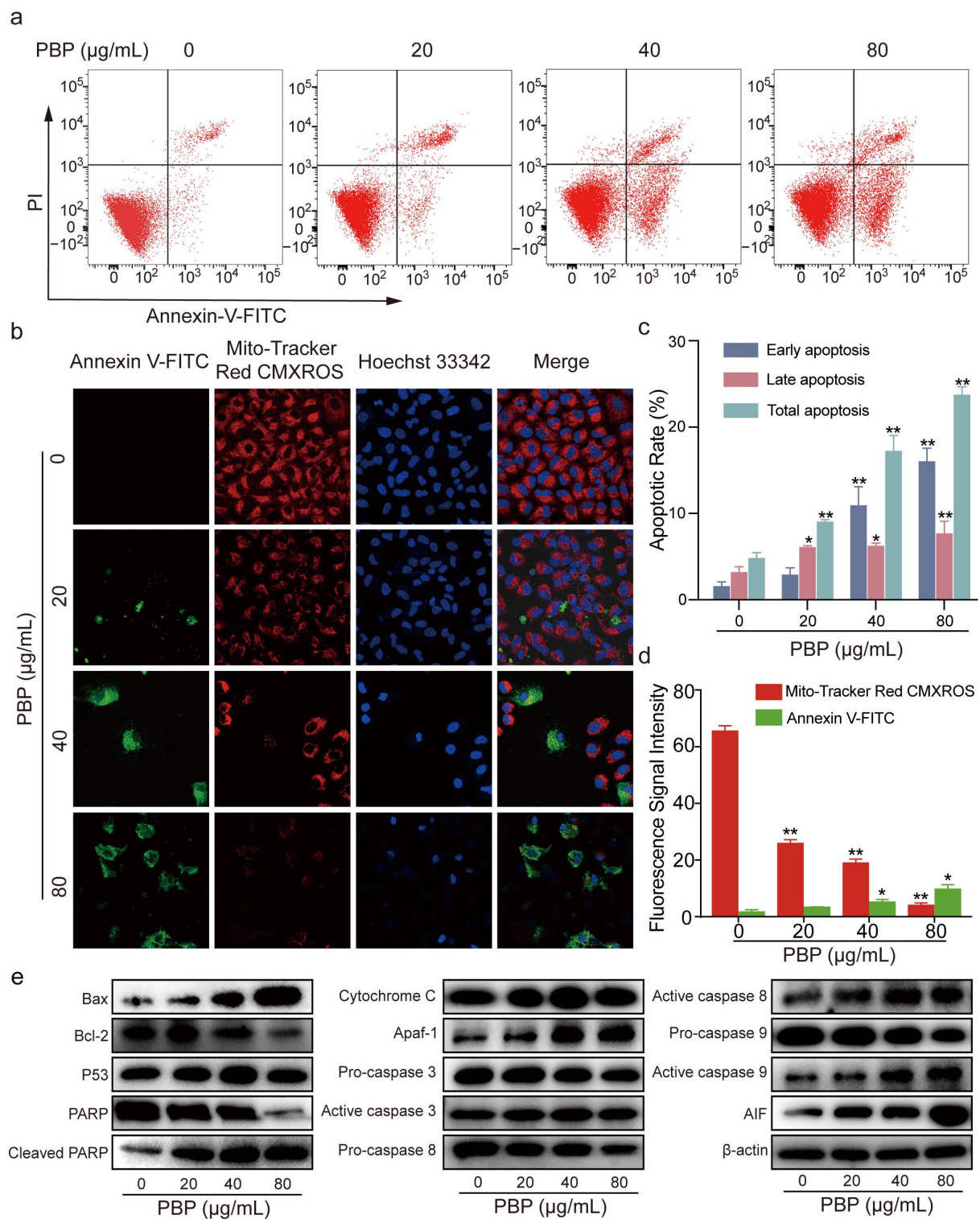


Figure 6. PBP induced apoptosis and caused MMP depolarization in A549 cells. (a) A549 cells were incubated with PBP (0, 20, 40 and 80 $\mu\text{g/mL}$) for 48 h and then stained with Annexin V-FITC and PI for evaluation by flow cytometry; (b) The MitoTracker Red CMXRos fluorescent probe was used to detect the MMP in A549 cells using a mitochondrial membrane potential detection kit and laser confocal microscopy; (c) Histograms of the apoptotic rates of A549 cells treated with PBP; (d) Histograms were used to determine the average fluorescence intensity; (e) Expression of apoptosis-related proteins was analyzed by western blot analysis. Data are presented as the mean \pm SD ($n = 3$) by One-way ANOVA analyses. ** $p < 0.01$, * $p < 0.05$ versus control (0 $\mu\text{g/mL}$ PBP).

The B-cell lymphoma-2 (Bcl-2) and Bax protein family regulates apoptosis and influences mitochondrial function [33]. Various downstream apoptotic mediators are activated and participate in a series of cell death cascade reactions. According to western blot analysis, PBP dose-dependently increased the proapoptotic protein Bax while downregulating the antiapoptotic regulator Bcl-2 (Figure 6e). Changes in Bcl-2 and Bax usually indicate that apoptosis occurs through the mitochondria-dependent apoptotic pathway. As a result, the expression levels of additional regulators involved in the mitochondrial apoptotic pathway were examined. The expression of P53, apoptosis inducing factor (AIF), apoptotic protease activating factor-1 (Apaf-1), Cytochrome C, active caspase-3, active caspase-9, and active caspase-8 were all enhanced by PBP, but inactive zymogen proteins including pro-caspase-9, pro-caspase-8, and pro-caspase-3 were decreased. Downregulated PARP expression and upregulated cleaved PARP expression also suggested that PBP promotes PARP cleavage in A549 cells (Figure 6e). These results suggest that PBP may release apoptosis activators by altering mitochondrial function, thereby activating the caspase pathway cascade. The upstream initiators pro-caspase-9 and pro-caspase-8 become activated to form active caspase-9 and active caspase-8, which in turn activate pro-caspase-3 to become active caspase-3, which acts as an executor to induce PARP cleavage, ultimately triggering endogenous apoptosis and DNA fragmentation. Protein expression histograms displaying the amounts of apoptosis-related proteins in Figure S2. As a result, PBP could cause apoptosis in A549 cells by activating the intrinsic apoptotic pathway of the mitochondria.

2.9. PBP Induced Mitochondrial Membrane Potential (MMP) Depolarization in A549 Cells

Apoptosis is associated with mitochondrial dysfunction and MMP depolarization [34]. We examined the changes in MMP using Mitochondrial Membrane Potential and Apoptosis Detection Kit. Annexin V⁻/CMXRos⁺ represents normal living cells. Annexin V⁺/CMXRos⁻ indicates cells with apoptosis and decreased mitochondrial membrane potential. The considerable decrease in fluorescence intensity of the Mito-Tracker Red CMXRos probe suggested that the number of A549 cells with normal MMP was dramatically decreased after treatment with PBP. The number of apoptotic cells labeled with the green fluorescent probe Annexin V-FITC increased significantly, again verifying that PBP treatment induced A549 cell apoptosis (Figure 6b,d). The blue fluorescent probe Hoechst 33342 was used for fluorescence detection. Compared to the control group, apoptotic cells with Annexin V⁺/CMXRos⁻ had smaller nuclei, and part of these nuclei had decomposed into fragments. According to these results, PBP-induced apoptosis in A549 cells may be related to MMP depolarization.

2.10. PBP Arrested the Cell Cycle of A549 Cells in S Phase

Following 48 h of PBP administration, 20,000 cells from each sample were gathered for flow cytometric analysis. The percent of A549 cells in S phase rose significantly after treatment with 80 g/mL PBP, rising from 9.35% ± 1.10% to 24.67% ± 0.33%, whereas the percentage in G1 stage decreased from 82.94% ± 1.43% to 67.90% ± 0.40%. However, PBP administration had no discernible impact on the percentage of A549 cells that were in the G2 phase (Figure 7a,c). These results suggested that PBP was able of S phase arrest in A549 cells.

Western blotting was used to confirm the expression levels of important cell cycle-related proteins. The results indicated that Rb was phosphorylated (P-Rb) under PBP treatment, resulting in increased release of free E2F transcription factor 1 (E2F1) from the E2F1/Rb complex. Similarly, PBP treatment inhibited Cyclin Dependent Kinase 2 (CDK2) and cyclin A2 and promoted P21 expression (Figure 7c). Protein expression histograms displaying the amounts of apoptosis-related proteins in Figure S3. The expression levels of the target proteins were normalized to those of β -actin. Therefore, PBP arrested A549 cells in S phase by altering the expression of key regulators, such as cyclin A2/CDK2, P21 and P53.

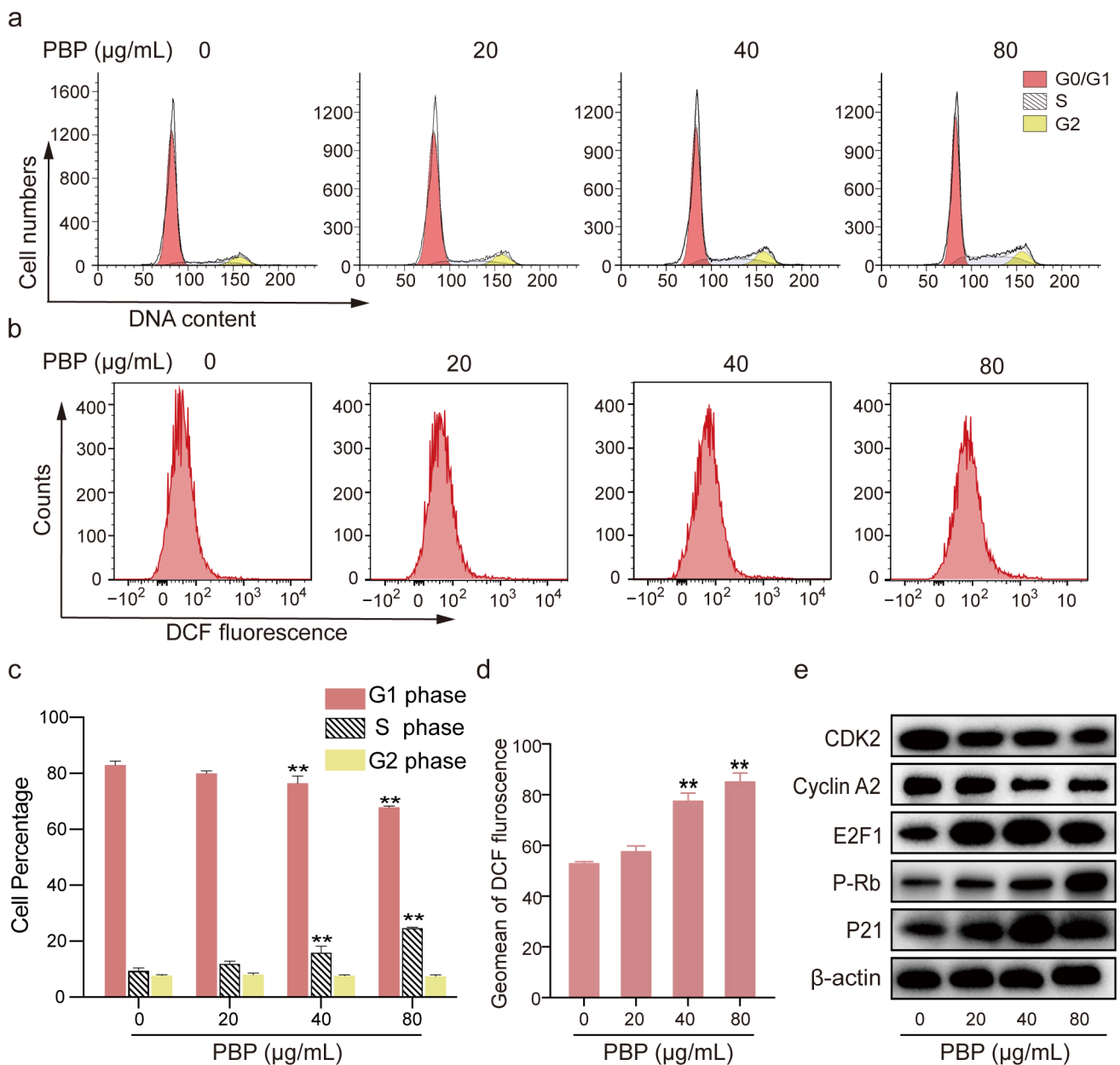


Figure 7. PBP arrested A549 cells in S phase and caused ROS production. (a) A549 cells were stained with PI and evaluated using flow cytometry after PBP (0, 20, 40 or 80 $\mu\text{g/mL}$) treatment for 48 h; (b) A549 cells were stained with the ROS indicator (DCF-DA) and analyzed by flow cytometry after PBP treatment for 48 h; (c) Analysis quantitative of the cell cycle distribution of A549 cells treated with PBP; (d) Quantitative analysis of the DCF fluorescence geomean in A549 cells treated with PBP; (e) Western blot analysis of proteins related to S phase arrest. Data are presented as the mean \pm SD ($n = 3$) by One-way ANOVA analyses. ** $p < 0.01$ versus control (0 $\mu\text{g/mL}$ PBP).

2.11. PBP Promoted Reactive Oxygen Species (ROS) Generation in A549 Cells

ROS are implicated in the apoptosis process [35,36]. The 10,000 cells were collected for each DCFH-DA staining sample after treatment with 0, 20, 40 and 80 $\mu\text{g/mL}$ PBP. Intracellular ROS can oxidize nonfluorescent DCFH to fluorescent DCF, which can be detected by flow cytometry [37]. The histograms of A549 cells shifted to the right when the PBP concentration increased. After treatment with 80 $\mu\text{g/mL}$ PBP, the geomean fluorescence intensity of DCF increased remarkably from 52.90 ± 1.56 to 85.13 ± 2.30 in A549 cells (Figure 7a,c). These results indicated that PBP-induced apoptosis may be associated with ROS production. that PBP-induced apoptosis could be associated with ROS production.

2.12. PBP Induced Mitochondrial Membrane Potential (MMP) Depolarization in A549 Cells

Apoptosis is associated with mitochondrial dysfunction and MMP depolarization [34]. We examined the changes in MMP using an MMP kit. The considerable decrease in fluorescence intensity of the MitoTracker Red CMXRos probe suggested that the number of A549 cells with normal MMP was dramatically decreased after treatment with PBP. The number of apoptotic cells labeled with the green fluorescent probe Annexin V-FITC increased significantly, again verifying that PBP treatment induced A549 cell apoptosis (Figure 7b,d). The blue fluorescent probe Hoechst 33342 was used for fluorescence detection. Compared to the control group, apoptotic cells without red fluorescence (MMP depolarization) but with green fluorescence (phosphatidylserine outside the cell membrane) had smaller nuclei, and part of these nuclei had decomposed into fragments. According to these results, PBP-induced apoptosis in A549 cells may be related to MMP depolarization.

3. Discussion

P. baumii, a traditional herbal medicine, has shown antitumor properties against a wide range of cancers [38]. Natural products are essential sources for the research and development of novel anticancer medicines. In this work, we determined the composition of PBP and identified its 17 chemical components and 2D structures, many of which have been proved to exert various pharmacological activities. For instance, hispidin induced apoptosis mediated by ROS in colon cancer cells, and could enhance the therapeutic activities of gemcitabine against pancreatic cancer stem cells [39,40].

Through the network pharmacology method, a total of 60 targets obtained by intersection were regarded as potential targets for PBP treatment of lung cancer. Protocatechuic aldehyde, caffeic acid, osmundacetone, hispidin, citrinin, davallialactone are considered to be potential bioactive compounds of PBP against lung cancer. GO and KEGG analysis showed the 33 of 61 (54%) intersection targets are related to apoptosis and cell cycle pathways (Figure 3). The results show that PBP may treat lung cancer by regulating apoptosis and cell cycle progression. Molecular docking elucidated the binding conformation and mechanism of the primary active components (Osmundacetone and hispidin) to the core targets CASP3, PARP1 and TP53 (Figure 4).

Apoptosis, a genetically regulated process of programmed cell death, has been acknowledged as a new cancer therapy [9,41]. In this study, typical apoptotic characteristics were seen in PBP-treated A549 cells, including cell volume shrinkage, detachment from the surrounding cells (Figure 5c), MMP depolarization (Figure 5b), positive Annexin V-FITC staining (Figure 5a,b). Other studies have shown that some bioactive substances in natural products exert antitumor effects mainly through three pathways, including the intrinsic mitochondrial pathway, extrinsic death receptor pathway and endoplasmic reticulum stress pathway [42]. Figure 5 indicated that PBP may induce apoptosis through mitochondrial department apoptosis pathways. The changes in Bcl-2 and Bax resulted in the disappearance of the MMP, therefore increasing the release of cytochrome C and AIF (Figure 5e), which activate a cascade of caspases. Active caspase-9 and active caspase-8 further activates downstream caspase-3, which acted as an executor to cleave PARP, resulting in irreparable DNA damage, thereby inducing apoptosis in A549 cells.

Therapeutics that target the cell cycle have emerged as a successful method for the treatment of cancer [43]. Cell cycle regulation is dependent on the cyclin family and CDK family of proteins. A reduction in or dysregulation of the cyclin A/CDK2 complex could cause cells to arrest in S phase. In this study, A549 cells treated with PBP were arrested in S phase (Figure 6a,e). Furthermore, PBP resulted in Rb phosphorylation (P-Rb), increasing the release of E2F1 from the E2F1/Rb complex. Moreover, PBP treatment inhibited CDK2 and cyclin A2 and promoted the expression of P21. These results suggest that inhibition of cyclin A2/CDK2 and upregulation of P21 and P53 play key roles in PBP-induced S-phase arrest in A549 cells (Figures 5e and 6e).

Previous studies have shown that ROS can be associated with a variety of cell cycle, apoptosis, autophagy pathway [44,45]. In this study, PBP induced ROS production and

MMP depolarization (Figure 5b), indicating that it is a potential factor to promote apoptosis and S phase arrest in A549 cells.

In conclusion, our investigations demonstrated that PBP exhibited remarkable anti-tumor capacities against lung cancer A549 cells in vitro. PBP induces apoptosis, cell cycle arrest, ROS accumulation and MMP depolarization in A549 cells (Figure 8). Moreover, the against lung cancer effects of PBP in vivo were not investigated in this work. However, it has been demonstrated that hot water extract of *Phellinus linteus* has been demonstrated to significantly suppress the S180 melanoma sarcoma and mouse colon cancer in vivo [46]. In addition, Jae-Sung Bae et al. found that polysaccharides isolated from *Phellinus gilvov* inhibit melanoma growth in mice [47]. What these in vivo studies have in common is that they all use intragastric administration. It is reasonable to speculate that the anti-tumor effect of *Phellinus linteus* is achieved by improving the changes of intestinal microflora, which deserves further consideration and research. These results in vivo suggest that PBP may have great potential for anti-tumor effects in vivo, including lung cancer. The polyphenol extract of *P. baumii* could be a potential candidate for future antitumor drug development, and it also lays a foundation for the study of the anti-tumor mechanism of *P. baumii* polyphenols.

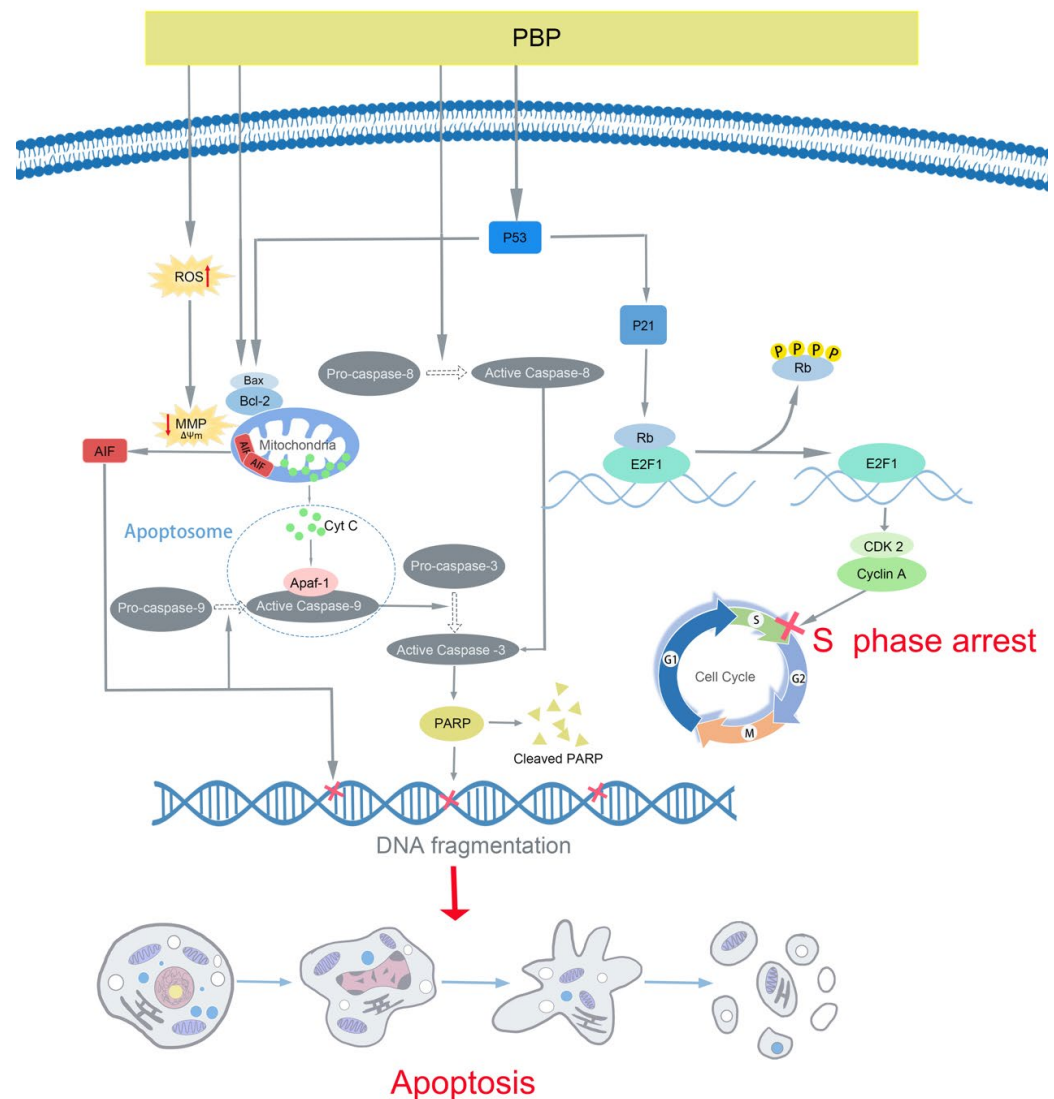


Figure 8. The potential mechanism of PBP exerted antitumor effect by inducing caspase-dependent mitochondrial intrinsic apoptotic pathway and arrested the cell cycle.

4. Materials and Methods

4.1. Reagents

Dulbecco's modified essential medium (DMEM, high glucose) and fetal bovine serum (FBS) were purchased from Gibco Industries Inc. (Grand Island, NY, USA). Dimethyl sulfoxide (DMSO) was purchased from Sigma—Aldrich (St. Louis, MO, USA). An Annexin V FITC apoptosis detection kit was obtained from Dojindo Molecular Technologies (Kumamoto, Japan). Trypsin (0.25% with or without EDTA), CCK-8, cell cycle detection kit and reactive oxygen species (ROS), Mitochondrial Membrane Potential Detection Kit (C1071; Beyotime, Shanghai, China) assay kit were purchased from Beyotime Institute of Biotechnology (Jiangsu, China). The fruiting bodies of *P. baumii* were obtained from Huqingyutang drugstore (Hangzhou, China).

HPLC-grade methanol was purchased from Sinopharm Chemical Reagent Co., Ltd. (Shanghai, China). Protocatechuic aldehyde, caffeic acid, osmundacetone and hispidin (all HPLC grade) were obtained from Weikeyi Biological Technology Co., Ltd. (Chengdu, China).

4.2. Preparation of PBP

The fruiting bodies of *P. baumii* were dried, ground, and passed through an 80-mesh sieve. The powder was suspended in 60% ethanol (1:60, *w/v*). After 30 min of ultrasound treatment, reflux extraction was performed at 90 °C for 1 h. The extract was subjected to vacuum filtration, and the filtrate was collected and centrifuged (10,000 rpm, 5 min). The solvent of the supernatant was evaporated at 40 °C in a rotary evaporator under low pressure and then the remaining material was lyophilized with a freeze dryer (LABCONCO, MO, USA). The crude ethanolic extract was purified with an AB-8 macroporous adsorption resin column (Solarbio, Beijing, China) eluted using distilled water, 30% ethanol and 70% ethanol in sequence. Then, the 70% ethanol eluent was collected, concentrated and lyophilized to obtain the purified PBP. The total polyphenol content of PBP was 94.47% ± 4.10%, as determined by the Folin-Ciocalteu (Solarbio, Beijing, China) method [48]. The obtained PBP powder was stored at 4 °C for the following experiments.

4.3. Identification of PBP Compounds by UPLC–ESI–QTOF–MS

PBP was dissolved in 80% methanol at a final concentration of 2 mg/mL. A Waters UPLC (Waters Corp., Milford, MA, USA) with a Waters ACQUITY UPLC HSS T3 column (150 mm × 3.0 mm i.d., 1.7 µm) was used in the assay at a temperature of 50 °C and flow rate of 0.3 mL/min. The injection volume of the sample was 3 µL, and the UV detector was set at 254 nm. The mobile phases were 0.1% formic acid-water (A) and 0.1% formic acid-acetonitrile (B). The linear gradient was as follows: 0/10, 2/20, 25/35, 35/95 (min/B%). Mass spectrometry was performed using an AB Triple TOF 5600 plus System (AB SCIEX, Framingham, USA). The optimal MS conditions were as follows: the scan ranges (*m/z*) of precursor ions and product ions were set as 100–1500 Da and 50–1500 Da, respectively; the source voltage and temperature for negative ion mode were –4.5 kV and 550 °C, respectively, and those for positive ion mode were +5.5 kV and 600 °C, respectively; the pressures of gas 1 (air) and gas 2 (air) were set to 50 psi, and that of the curtain gas (N₂) was set to 35 psi; the maximum permissible error was set to ± 5 ppm; and the declustering potential (DP) and collision energy (CE) were 100 V and 10 V, respectively. MS/MS acquisition was performed with almost the same parameters except that the CEs were set to –40 ± 20 V and 40 ± 20 V in negative and positive ion modes, respectively. The mass axis was calibrated with a CDS pump to reduce the mass axis error to less than 2 ppm.

The data were analyzed with PeakView 1.2 software (ABSciex, Vaughan, ON, Canada). A compound library of polyphenol constituents previously discovered in *Phellinus* spp. was constructed to help with identification. Published research and chemical databases, such as Reaxys, PubChem, and ChemSpider, also helped with the identification of these compounds.

4.4. Prediction of Potential Targets of PBP during Lung Cancer Treatment

Potential targets information of 17 active compounds of PBP were collected from TCMSP database (<https://old.tcmsp-e.com/tcmsp.php> (accessed on 10 November 2022)) [49] and Drugbank database (<https://go.drugbank.com/> (accessed on 10 November 2022)) [50]. Lung cancer-treat targets were collected from 4 databases using the keyword 'lung cancer': GeneCards database (<https://www.genecards.org/> ((accessed on 10 November 2022))) [51], Human Online Mendelian Inheritance database (OMIM, <https://www.omim.org/> ((accessed on 10 November 2022))) [52], DisGeNET database (<https://www.disgenet.org/> ((accessed on 10 November 2022))) [53] and TTD (<http://db.idrblab.net/ttd> ((accessed on 10 November 2022))) [54]. The intersection of PBP active component targets and lung cancer-related targets is regarded as the potential targets for PBP treatment of lung cancer. Visualization using Venny 2.1 (<https://bioinfogp.cnb.csic.es/tools/venny> ((accessed on 10 November 2022))).

4.5. Component-Disease-Target Interaction Network

The potential targets of active compounds in PBP were constructed as a Drug-Component-Disease-Target visual interaction network using Cytoscape 3.9.1 software [55]. Compounds with more than the mean of degree centrality are considered core compounds.

4.6. GO and KEGG Enrichment Analysis

DAVID database (<https://david.ncifcrf.gov/> ((accessed on 10 November 2022))) [56] was used to further analyze the potential targets of PBP in the treatment of lung cancer. We used DAVID to analyze the biological process (BP), cellular component (CC), and molecular function (MF) terms of the common targets. The main pathways that were enriched were subsequently examined using the KEGG database (<https://www.kegg.jp/> ((accessed on 10 November 2022))) [57]. The KEGG pathways and GO terms were determined with $p < 0.05$.

4.7. PPI Network and Core Targets

The PBP treatment of lung cancer intersection targets were analyzed by STRING database (<https://string-db.org/> ((accessed on 10 November 2022))) [58]. The species was set to 'homo', the confidence score was set to >0.9 to obtain a more relevant protein interaction network. The visualized PPI network and topological values was constructed by Cytoscape 3.9.1. Targets that simultaneously satisfy the mean values of degree centrality (DC), betweenness centrality (BC), and closeness centrality (CC) were identified as core targets.

4.8. Molecular Docking

The 3D chemical structures of the PBP components were obtained from the PubChem database (<https://pubchem.ncbi.nlm.nih.gov/> ((accessed on 10 November 2022))). The 3D structures of the core targets from the protein database (PDB, <https://www.rcsb.org/> ((accessed on 10 November 2022))) [59]. Autodock 4, Autodock Tools 1.5.7 and Autodock Vina [60] are used to detect and select rotatable bonds in compounds, remove water, add hydrogen from protein 3D structures. Then, Autodock Vina was used for molecular docking of PBP compounds with the core targets. The binding activity between each component and the target was evaluated according to the binding energy, the affinity < -5 kcal/mol was defined as a good binding activity. PyMOL software was used for analysis and plotting.

4.9. Cell Lines and Culture

Human lung cancer A549 cell line (RRID: CVCL_0023) and human embryonic kidney HEK293 cell line (RRID: CVCL_0045) were obtained from the Cell Research Institute of the Chinese Academy of Sciences (Shanghai, China). The cells used in the experiment were 6–10 generation cell lines. The cells were cultured in DMEM (high glucose) supplemented with 10% (*v/v*) FBS at 37 °C under a humid atmosphere with 5% CO₂.

4.10. Cell Viability Assay and Morphological Observations

Cells (5×10^3 cells/well) were seeded in 96-well plates (Costar Corning, Rochester, NY, USA), cultured for 24 h to allow for adherence, and then treated with PBP for 24, 48 and 72 h. After that, 10 μ L of CCK-8 solution was added to each well, and the incubation continued for 2 h at 37 °C. The absorbance was measured using a multimode reader (Thermo Electron Corporation, MA, USA) at 450 nm. The wells without cells but with all other reagents were used as the blank, and the cell viability rate was calculated as follows:

$$\text{Cell Viability (\%)} = (A_{450 \text{ treated}} - A_{450 \text{ blank}}) / (A_{450 \text{ Control}} - A_{450 \text{ blank}}) \times 100\%$$

The cell morphology was observed and photographed by an Olympus phase contrast microscope (Olympus, Tokyo, Japan).

4.11. Cell Apoptosis Assay

Cell apoptosis was determined using an Annexin V, FITC Apoptosis Detection Kit and flow cytometer. A549 cells were seeded in 6-well plates at 1×10^5 cells/well. After 24 h of culture, the cells were treated with PBP (0, 20, 40, 80 μ g/mL) for 48 h. Then, the cells were digested, washed and stained with Annexin V-FITC (5 μ L/well) and PI (5 μ L/well), incubated for 15 min in the dark, and analyzed on a BD FACSVerser flow cytometer. The cell apoptosis rate data were analyzed using FlowJo software.

4.12. MMP Assay

The membrane potential was determined by using a Mitochondrial Membrane Potential and Apoptosis Detection Kit with Mito-Tracker Red CMXRos and Annexin V-FITC (C1071; Beyotime, Shanghai, China). Cells were seeded into 6-well plates (1×10^5 cells/well) and cultured for 24 h. After 48 h of incubation with PBP, the cell culture medium was removed by aspiration and the cells were washed once with PBS. Then, Annexin V-FITC binding solution (188 μ L/plate), Annexin V-FITC (5 μ L/plate), MitoTracker Red CMXRos staining solution (2 μ L/plate), and Hoechst 33342 staining solution (5 μ L/plate) were added. The samples were incubated in the dark for 20–30 min at room temperature and then placed in an ice bath. The sample smears were visualized under a laser confocal microscope (Leica Microsystems, Wetzlar, Germany).

4.13. Western Blot Assay

Cells were seeded into 6-well plates (1×10^5 cells/well) and cultured for 24 h. After treatment with PBP (20, 40, 80 μ g/mL) for 48 h, the total proteins were extracted by Cell lysis buffer for Western and IP (Beyotime, Shanghai, China). The concentrations of extracted protein were determined by using a BCA protein assay kit (Beyotime, Shanghai, China). Proteins were loaded into each well of a 10% or 15% sodium dodecyl sulfate—polyacrylamide gel electrophoresis (SDS—PAGE) and then transferred to a polyvinylidene difluoride (PVDF) membrane. After blocking with 5% nonfat dry milk with 0.05% Tween 20 in TBS (1 \times) for 1 h at 25 °C, the membranes were incubated with the corresponding primary antibodies at 4 °C overnight. The primary antibodies were rabbit anti-human P53 (E26, Abcam, Cambridge, UK), β -actin (R1207-1, HUABIO, Woburn, MA, USA), AIF (ET1603-4, HUABIO), Bcl-2 (ER0602, HUABIO), Bax (ET1603-34, HUABIO), Apaf-1 (R1312-20, HUABIO), poly ADP-ribose polymerase (PARP, ET1608-56, HUABIO), cleaved PARP (ET1608-10, HUABIO), CDK2 (ET1602-6, HUABIO), phosphorylated retinoblastoma protein (P-Rb, ET1602-36, HUABIO), cyclin A2(ET1612-26, HUABIO), E2F transcription factor 1 (E2F1, ET1701-73, HUABIO), active + pro caspase 9 (R1308-12, HUABIO), caspase-3 (ET1602-39, HUABIO), active caspase-3 (ET1602-47, HUABIO), caspase-8 (ET1603-16, HUABIO), cytochrome C(ET1610-60, HUABIO). The membranes were then incubated with secondary antibodies, HRP Conjugated Goat anti-Rabbit IgG (HUABIO, Hangzhou, China), at room temperature for 1 h. Protein signals were visualized by Enhanced ECL Chemiluminescent Substrate Kit (Yeasen, Shanghai, China).

4.14. Cell Cycle Assay

Cell cycle analysis was conducted by flow cytometry. Cells were seeded into 6-well plates (2×10^5 cells/well) and cultured for 24 h. After treatment with PBP for 48 h, the cells were digested with trypsin, rinsed twice with cold phosphate-buffered saline (PBS), fixed with 70% precooled ethanol and washed three times with PBS. Then, the cells were incubated with PI staining solution containing RNase A at 37 °C for 1.5 h. Cell cycle analysis was conducted on a BD FACSVerser flow cytometer and analyzed with Modfit LT software.

4.15. ROS Generation Assay

Cells were seeded into 6-well plates (1×10^5 cells/well) and cultured for 24 h. After 48 h of incubation with PBP, the cells were collected and washed twice with PBS. Then, the cells were incubated with DCFH-DA at 37 °C for 20 min, rinsed twice and resuspended in DMEM. The ROS levels in the cells were determined with a BD FACSVerser flow cytometer and the data were analyzed by FlowJo software.

4.16. Statistical Analysis

Statistical analyses were performed using GraphPad Prism software version 8.0.2 (GraphPad, San Diego, CA, USA). The statistical significance of the differences between groups was analyzed by one-way ANOVA with Dunnett's test as a post hoc analysis. Data are presented as the mean \pm SD. Differences with a p value < 0.05 or p value < 0.01 were considered statistically significant or extremely significant, respectively. The flow cytometry gating strategy is shown in (Figure A2).

Supplementary Materials: The following supporting information can be downloaded at: <https://www.mdpi.com/article/10.3390/ijms232416141/s1>.

Author Contributions: All authors contributed to the study conception and design. Conceptualization, L.S., X.L. and S.C. Material preparation, experimental design and experimental operation, and data analysis were performed by X.L. and S.C. The first draft of the manuscript was written by X.L., S.C. and all authors C.D., W.L., H.X., C.L. commented on previous versions of the manuscript. All authors have read and agreed to the published version of the manuscript.

Funding: This research was funded by National Natural Science Foundation of China (32170482), Science and Technology Correspondent Team Project of Zhejiang Province Grants (20191026).

Institutional Review Board Statement: Not applicable.

Informed Consent Statement: Not applicable.

Data Availability Statement: Not applicable.

Acknowledgments: We are grateful to Zhi-Wei Ge (Analysis Center for Agrobiolgy and Environmental Sciences, Zhejiang University) for the help of UPLC-ESI-QTOF-MS. And we are grateful to Zongpu Xu is appreciated for the guidance on writing.

Conflicts of Interest: The authors declare no conflict of interest.

Abbreviations

| | |
|--------|--|
| AIF | Apoptosis Inducing Factor |
| Apaf-1 | Apoptotic Protease Activating Factor-1 |
| Bcl-2 | B-cell lymphoma-2 |
| BC | betweenness centrality |
| CC | closeness centrality |
| CCK-8 | Cell Counting Kit-8 |
| CDK2 | Cyclin Dependent Kinase 2 |
| CVD | cardiovascular diseases |

| | |
|------------------|---|
| DC | degree centrality |
| DMEM | dulbecco's modified essential medium |
| DMSO | Di-methyl sulfoxide |
| E2F1 | E2F transcription factor 1 |
| FBS | fetal bovine serum |
| GO | Gene ontology |
| KEGG | kyoto encyclopedia of genes and genomes |
| MMP | mitochondrial membrane potential |
| P-Rb | Phosphorylated Retinoblastoma protein |
| PARP | Poly ADP-Ribose Polymerase |
| PBP | Phellinus baumii polyphenol |
| PPI | Protein-protein interaction |
| PVDF | polyvinylidene difluoride |
| ROS | reactive oxygen species |
| SDS—PAGE | sulfate—polyacrylamide gel electrophoresis |
| TCMSP | traditional chinese medicine systems pharmacology database and analysis platform |
| TTD | treatment targets database |
| UPLC-ESI-QTOF-MS | Ultra Performance Liquid Chromatography-Electrospray Ionization-Quadrupole Time of Flight-Mass Spectrometry |

Appendix A

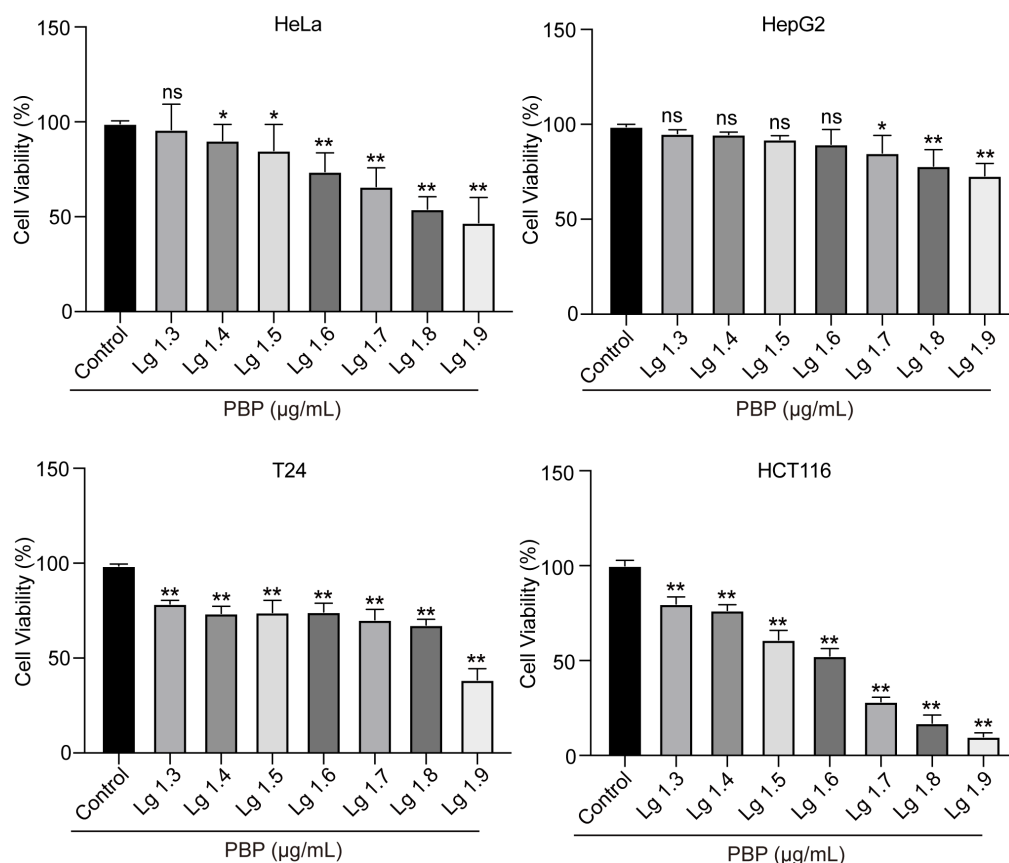


Figure A1. Cytotoxicity of PBP to HeLa, HepG2, T24 and HCT116 human tumor cells using the CCK-8 assay, after being exposed to varying amounts of PBP for 48 h. Data are presented as the mean \pm SD ($n = 3$) by One-way ANOVA analyses. ** $p < 0.01$, * $p < 0.05$ versus control (0 $\mu\text{g/mL}$ PBP).

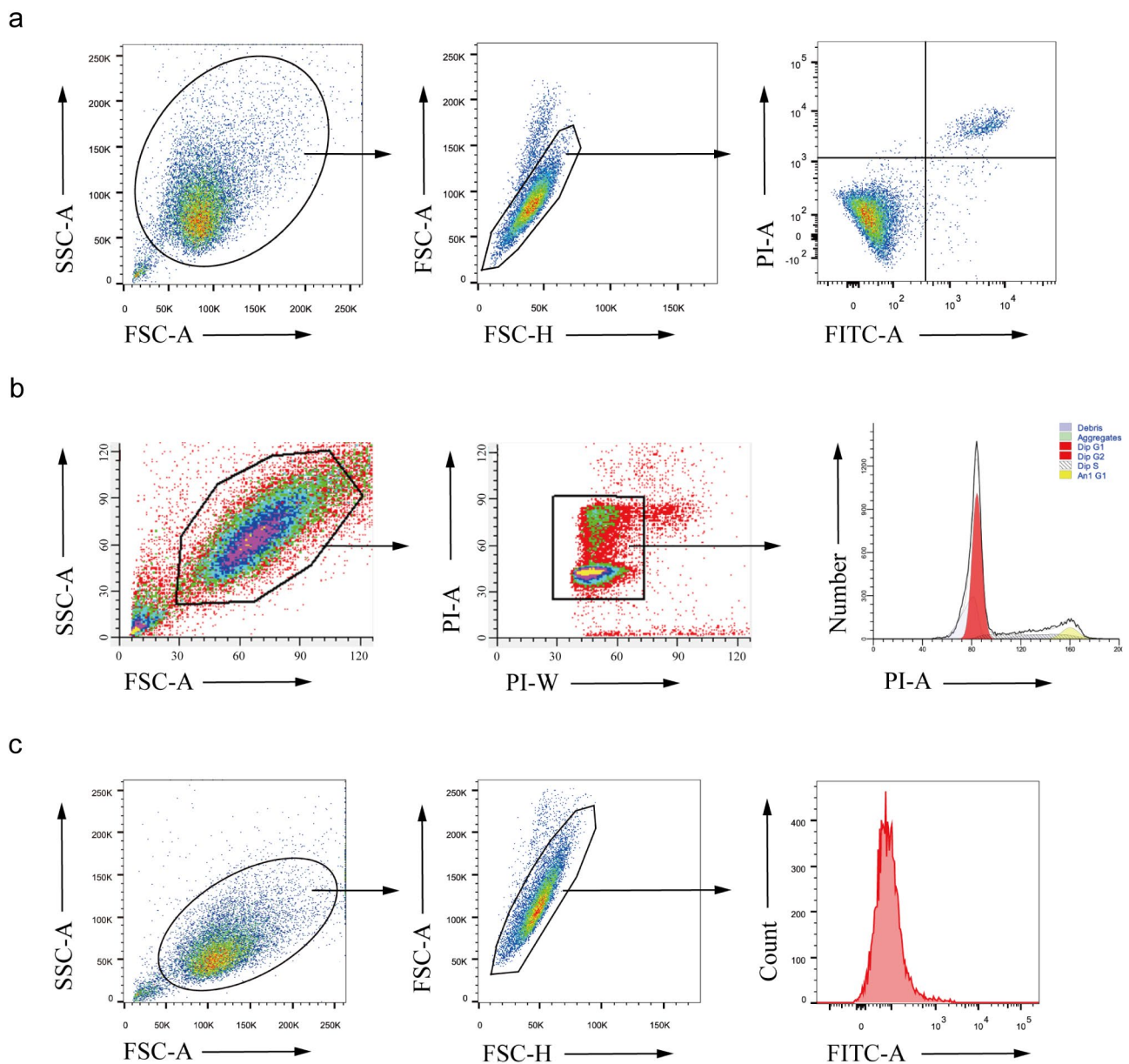


Figure A2. Flow cytometry gating strategy. (a) To determine cell apoptosis induced by PBP, cells were gated on FSC-A/SSC-A, FSC-H/FSC-A and then FITC-A/PI-A events to reduce the influence of cell debris and masses of dead cells. Viable cells, early apoptosis cells and late apoptosis cells were respectively defined as FITC-PI-, FITC+PI- and FITC+PI+; (b) Cells were gated on FSC-A/SSC-A and PI-W/PI-A events using Modfit LT software for cell cycle analysis; (c) Cells were gated on FSC-A/SSC-A and FSC-H/FSC-A events for ROS determination.

References

1. Sung, H.; Ferlay, J.; Siegel, R.L.; Laversanne, M.; Soerjomataram, I.; Jemal, A.; Bray, F. Global Cancer Statistics 2020: GLOBOCAN Estimates of Incidence and Mortality Worldwide for 36 Cancers in 185 Countries. *CA Cancer J. Clin.* **2021**, *71*, 209–249. [[CrossRef](#)] [[PubMed](#)]
2. Niedzwiecki, A.; Roomi, M.W.; Kalinovsky, T.; Rath, M. Anticancer Efficacy of Polyphenols and Their Combinations. *Nutrients* **2016**, *8*, 552. [[CrossRef](#)] [[PubMed](#)]
3. Zhou, Y.; Zheng, J.; Li, Y.; Xu, D.P.; Li, S.; Chen, Y.M.; Li, H.B. Natural Polyphenols for Prevention and Treatment of Cancer. *Nutrients* **2016**, *8*, 515. [[CrossRef](#)] [[PubMed](#)]
4. Yi, J.; Qu, H.; Wu, Y.; Wang, Z.; Wang, L. Study on antitumor, antioxidant and immunoregulatory activities of the purified polyphenols from pinecone of *Pinus koraiensis* on tumor-bearing S180 mice in vivo. *Int. J. Biol. Macromol.* **2017**, *94*, 735–744. [[CrossRef](#)] [[PubMed](#)]

5. Yang, C.S.; Wang, X.; Lu, G.; Picinich, S.C. Cancer prevention by tea: Animal studies, molecular mechanisms and human relevance. *Nat. Rev. Cancer* **2009**, *9*, 429–439. [[CrossRef](#)]
6. Sinha, D.; Sarkar, N.; Biswas, J.; Bishayee, A. Resveratrol for breast cancer prevention and therapy: Preclinical evidence and molecular mechanisms. *Semin. Cancer Biol.* **2016**, *40–41*, 209–232. [[CrossRef](#)]
7. Zhang, Q.; Huang, H.; Zheng, F.; Liu, H.; Qiu, F.; Chen, Y.; Liang, C.L.; Dai, Z. Resveratrol exerts antitumor effects by downregulating CD8(+)CD122(+) Tregs in murine hepatocellular carcinoma. *Oncimmunology* **2020**, *9*, 1829346. [[CrossRef](#)]
8. He, P.; Zhang, Y.; Li, N. The phytochemistry and pharmacology of medicinal fungi of the genus *Phellinus*: A review. *Food Funct.* **2021**, *12*, 1856–1881. [[CrossRef](#)]
9. Liu, M.M.; Zeng, P.; Li, X.T.; Shi, L.G. Antitumor and immunomodulation activities of polysaccharide from *Phellinus baumii*. *Int. J. Biol. Macromol.* **2016**, *91*, 1199–1205. [[CrossRef](#)]
10. Li, G.; Kim, D.H.; Kim, T.D.; Park, B.J.; Park, H.D.; Park, J.I.; Na, M.K.; Kim, H.C.; Hong, N.D.; Lim, K.; et al. Protein-bound polysaccharide from *Phellinus linteus* induces G2/M phase arrest and apoptosis in SW480 human colon cancer cells. *Cancer Lett.* **2004**, *216*, 175–181. [[CrossRef](#)]
11. Sun, Y.; Huo, J.; Zhong, S.; Zhu, J.; Li, Y.; Li, X. Chemical structure and anti-inflammatory activity of a branched polysaccharide isolated from *Phellinus baumii*. *Carbohydr. Polym.* **2021**, *268*, 118214. [[CrossRef](#)]
12. Feng, H.; Zhang, S.; Wan, J.M.; Gui, L.; Ruan, M.; Li, N.; Zhang, H.; Liu, Z.; Wang, H. Polysaccharides extracted from *Phellinus linteus* ameliorate high-fat high-fructose diet induced insulin resistance in mice. *Carbohydr. Polym.* **2018**, *200*, 144–153. [[CrossRef](#)]
13. Wang, G.J.; Tsai, T.H.; Chang, T.T.; Chou, C.J.; Lin, L.C. Lanostanes from *Phellinus igniarius* and their iNOS inhibitory activities. *Planta Med.* **2009**, *75*, 1602–1607. [[CrossRef](#)]
14. Jang, H.J.; Yang, K.S. Inhibition of nitric oxide production in RAW 264.7 macrophages by diterpenoids from *Phellinus pini*. *Arch. Pharm. Res.* **2011**, *34*, 913–917. [[CrossRef](#)]
15. Zhang, H.; Chen, R.; Zhang, J.; Bu, Q.; Wang, W.; Liu, Y.; Li, Q.; Guo, Y.; Zhang, L.; Yang, Y. The integration of metabolome and proteome reveals bioactive polyphenols and hispidin in ARTP mutagenized *Phellinus baumii*. *Sci. Rep.* **2019**, *9*, 16172. [[CrossRef](#)]
16. Yang, K.; Zhang, S.; Geng, Y.; Tian, B.; Cai, M.; Guan, R.; Li, Y.; Ye, B.; Sun, P. Anti-Inflammatory Properties In Vitro and Hypoglycaemic Effects of Phenolics from Cultivated Fruit Body of *Phellinus baumii* in Type 2 Diabetic Mice. *Molecules* **2021**, *26*, 2285. [[CrossRef](#)]
17. Zheng, S.; Deng, S.; Huang, Y.; Huang, M.; Zhao, P.; Ma, X.; Wen, Y.; Wang, Q.; Yang, X. Anti-diabetic activity of a polyphenol-rich extract from *Phellinus igniarius* in KK-Ay mice with spontaneous type 2 diabetes mellitus. *Food Funct.* **2018**, *9*, 614–623. [[CrossRef](#)]
18. Nogales, C.; Mamdouh, Z.M.; List, M.; Kiel, C.; Casas, A.I.; Schmidt, H. Network pharmacology: Curing causal mechanisms instead of treating symptoms. *Trends Pharmacol. Sci.* **2022**, *43*, 136–150. [[CrossRef](#)]
19. Wu, C.S.; Lin, Z.M.; Wang, L.N.; Guo, D.X.; Wang, S.Q.; Liu, Y.Q.; Yuan, H.Q.; Lou, H.X. Phenolic compounds with NF-kappaB inhibitory effects from the fungus *Phellinus baumii*. *Bioorg. Med. Chem. Lett.* **2011**, *21*, 3261–3267. [[CrossRef](#)]
20. Dong, Y.; Qiu, P.; Zhu, R.; Zhao, L.; Zhang, P.; Wang, Y.; Li, C.; Chai, K.; Shou, D.; Zhao, H. A Combined Phytochemistry and Network Pharmacology Approach to Reveal the Potential Antitumor Effective Substances and Mechanism of *Phellinus igniarius*. *Front. Pharmacol.* **2019**, *10*, 266. [[CrossRef](#)]
21. Jung, J.Y.; Lee, I.K.; Seok, S.J.; Lee, H.J.; Kim, Y.H.; Yun, B.S. Antioxidant polyphenols from the mycelial culture of the medicinal fungi *Inonotus xeranticus* and *Phellinus linteus*. *J. Appl. Microbiol.* **2008**, *104*, 1824–1832. [[CrossRef](#)]
22. Suabjakyong, P.; Saiki, R.; Van Griensven, L.J.; Higashi, K.; Nishimura, K.; Igarashi, K.; Toida, T. Polyphenol extract from *Phellinus igniarius* protects against acrolein toxicity in vitro and provides protection in a mouse stroke model. *PLoS ONE* **2015**, *10*, e0122733. [[CrossRef](#)]
23. Wang, Y.; Wang, S.J.; Mo, S.Y.; Li, S.; Yang, Y.C.; Shi, J.G. Phelligridimer A, a highly oxygenated and unsaturated 26-membered macrocyclic metabolite with antioxidant activity from the fungus *Phellinus igniarius*. *Org. Lett.* **2005**, *7*, 4733–4736. [[CrossRef](#)]
24. Lee, Y.S.; Kang, Y.H.; Jung, J.Y.; Kang, I.J.; Han, S.N.; Chung, J.S.; Shin, H.K.; Lim, S.S. Inhibitory constituents of aldose reductase in the fruiting body of *Phellinus linteus*. *Biol. Pharm. Bull.* **2008**, *31*, 765–768. [[CrossRef](#)]
25. Ding, Y.Y.; Liu, F.; Shi, C.; Zhang, Y.; Li, N. Chemical constituents from *Phellinus igniarius* and their anti-tumor activity in vitro. *Zhongguo Zhong Yao Za Zhi* **2016**, *41*, 3042–3048. [[CrossRef](#)]
26. Wang, Y.; Shang, X.Y.; Wang, S.J.; Mo, S.Y.; Li, S.; Yang, Y.C.; Ye, F.; Shi, J.G.; He, L. Structures, biogenesis, and biological activities of pyrano [4,3-c]isochromen-4-one derivatives from the Fungus *Phellinus igniarius*. *J. Nat. Prod.* **2007**, *70*, 296–299. [[CrossRef](#)]
27. Lee, I.K.; Yun, B.S. Styrylpyrone-class compounds from medicinal fungi *Phellinus* and *Inonotus* spp., and their medicinal importance. *J. Antibiot.* **2011**, *64*, 349–359. [[CrossRef](#)]
28. Saraiva, L.; Fresco, P.; Pinto, E.; Sousa, E.; Pinto, M.; Goncalves, J. Inhibition of alpha, beta, delta, eta, and zeta protein kinase C isoforms by xanthonolignoids. *J. Enzyme Inhib. Med. Chem.* **2003**, *18*, 357–370. [[CrossRef](#)]
29. Fischer, W.; Currais, A.; Liang, Z.; Pinto, A.; Maher, P. Old age-associated phenotypic screening for Alzheimer's disease drug candidates identifies sterubin as a potent neuroprotective compound from Yerba santa. *Redox Biol.* **2019**, *21*, 101089. [[CrossRef](#)]
30. He, W.; Wang, J.; Jin, Q.; Zhang, J.; Liu, Y.; Jin, Z.; Wang, H.; Hu, L.; Zhu, L.; Shen, M.; et al. Design, green synthesis, antioxidant activity screening, and evaluation of protective effect on cerebral ischemia reperfusion injury of novel monoene monocarbonyl curcumin analogs. *Bioorg. Chem.* **2021**, *114*, 105080. [[CrossRef](#)]

31. de Carvalho, J.T.G.; Da Silva Baldivia, D.; de Castro, D.T.H.; Dos Santos, H.F.; Dos Santos, C.M.; Oliveira, A.S.; Alfredo, T.M.; Vilharva, K.N.; de Picoli Souza, K.; Dos Santos, E.L. The immunoregulatory function of polyphenols: Implications in cancer immunity. *J. Nutr. Biochem.* **2020**, *85*, 108428. [[CrossRef](#)]
32. Elenkov, I.J.; Hrvacic, B.; Markovic, S.; Mesic, M.; Klonkay, A.C.; Lerman, L.; Sucic, A.F.; Vujasinovic, I.; Bosnjak, B.; Brajsa, K.; et al. Synthesis and Anti-inflammatory Activity of Novel Furochromenes. *Croat. Chem. Acta* **2013**, *86*, 253–264. [[CrossRef](#)]
33. Tsujimoto, Y. Role of Bcl-2 family proteins in apoptosis: Apoptosomes or mitochondria? *Genes Cells* **1998**, *3*, 697–707. [[CrossRef](#)]
34. Daugas, E.; Susin, S.A.; Zamzami, N.; Ferri, K.F.; Irinopoulou, T.; Larochette, N.; Prévost, M.C.; Leber, B.; Andrews, D.; Penninger, J.; et al. Mitochondrio-nuclear translocation of AIF in apoptosis and necrosis. *FASEB J.* **2000**, *14*, 729–739. [[CrossRef](#)]
35. Circu, M.L.; Aw, T.Y. Reactive oxygen species, cellular redox systems, and apoptosis. *Free Radic. Biol. Med.* **2010**, *48*, 749–762. [[CrossRef](#)]
36. Gorrini, C.; Harris, I.S.; Mak, T.W. Modulation of oxidative stress as an anticancer strategy. *Nat. Rev. Drug Discov.* **2013**, *12*, 931–947. [[CrossRef](#)]
37. Tie, F.; Li, G.; Hu, N.; Li, J.; Wang, Z.; Wang, H. Oligostilbenes extracts from *Iris lactea* Pall. var. *chinensis* (Fisch.) Koidz improve lipid metabolism in HFD/STZ-induced diabetic mice and inhibit adipogenesis in 3T3-L1 cells. *Biomed. Pharmacother.* **2020**, *131*, 110800. [[CrossRef](#)]
38. Sarfraz, A.; Rasul, A.; Sarfraz, I.; Shah, M.A.; Hussain, G.; Shafiq, N.; Masood, M.; Adem, S.; Sarker, S.D.; Li, X. Hispolon: A natural polyphenol and emerging cancer killer by multiple cellular signaling pathways. *Environ. Res.* **2020**, *190*, 110017. [[CrossRef](#)]
39. Lim, J.H.; Lee, Y.M.; Park, S.R.; Kim, D.H.; Lim, B.O. Anticancer activity of hispidin via reactive oxygen species-mediated apoptosis in colon cancer cells. *Anticancer Res.* **2014**, *34*, 4087–4093.
40. Chandimali, N.; Huynh, D.L.; Jin, W.Y.; Kwon, T. Combination Effects of Hispidin and Gemcitabine via Inhibition of Stemness in Pancreatic Cancer Stem Cells. *Anticancer Res.* **2018**, *38*, 3967–3975. [[CrossRef](#)]
41. Elmore, S. Apoptosis: A review of programmed cell death. *Toxicol. Pathol.* **2007**, *35*, 495–516. [[CrossRef](#)]
42. Kondo, S. Apoptosis by antitumor agents and other factors in relation to cell cycle checkpoints. *J. Radiat Res.* **1995**, *36*, 56–62. [[CrossRef](#)]
43. Ingham, M.; Schwartz, G.K. Cell-Cycle Therapeutics Come of Age. *J. Clin. Oncol.* **2017**, *35*, 2949–2959. [[CrossRef](#)]
44. Han, Y.; Ishibashi, S.; Iglesias-Gonzalez, J.; Chen, Y.; Love, N.R.; Amaya, E. Ca(2+)-Induced Mitochondrial ROS Regulate the Early Embryonic Cell Cycle. *Cell. Rep.* **2018**, *22*, 218–231. [[CrossRef](#)]
45. Wang, Z.; Yin, F.; Xu, J.; Zhang, T.; Wang, G.; Mao, M.; Wang, Z.; Sun, W.; Han, J.; Yang, M.; et al. CYT997(Lexibulin) induces apoptosis and autophagy through the activation of mutually reinforced ER stress and ROS in osteosarcoma. *J. Exp. Clin. Cancer Res.* **2019**, *38*, 44. [[CrossRef](#)]
46. Fang, J.; Gao, S.; Islam, R.; Teramoto, Y.; Maeda, H. Extracts of *Phellinus linteus*, Bamboo (*Sasa senanensis*) Leaf and Chaga Mushroom (*Inonotus obliquus*) Exhibit Antitumor Activity through Activating Innate Immunity. *Nutrients* **2020**, *12*, 2279. [[CrossRef](#)]
47. Bae, J.S.; Jang, K.H.; Yim, H.; Jin, H.K. Polysaccharides isolated from *Phellinus gilvus* inhibit melanoma growth in mice. *Cancer Lett.* **2005**, *218*, 43–52. [[CrossRef](#)]
48. Ainsworth, E.A.; Gillespie, K.M. Estimation of total phenolic content and other oxidation substrates in plant tissues using Folin-Ciocalteu reagent. *Nat. Protoc.* **2007**, *2*, 875–877. [[CrossRef](#)]
49. Ru, J.; Li, P.; Wang, J.; Zhou, W.; Li, B.; Huang, C.; Li, P.; Guo, Z.; Tao, W.; Yang, Y.; et al. TCMSP: A database of systems pharmacology for drug discovery from herbal medicines. *J. Cheminform.* **2014**, *6*, 13. [[CrossRef](#)]
50. Wishart, D.S.; Feunang, Y.D.; Guo, A.C.; Lo, E.J.; Marcu, A.; Grant, J.R.; Sajed, T.; Johnson, D.; Li, C.; Sayeeda, Z.; et al. DrugBank 5.0: A major update to the DrugBank database for 2018. *Nucleic Acids Res.* **2018**, *46*, D1074–D1082. [[CrossRef](#)]
51. Rebhan, M.; Chalifa-Caspi, V.; Prilusky, J.; Lancet, D. GeneCards: Integrating information about genes, proteins and diseases. *Trends Genet.* **1997**, *13*, 163. [[CrossRef](#)]
52. Hamosh, A.; Amberger, J.S.; Bocchini, C.; Scott, A.F.; Rasmussen, S.A. Online Mendelian Inheritance in Man (OMIM®): Victor McKusick’s magnum opus. *Am. J. Med. Genet. A* **2021**, *185*, 3259–3265. [[CrossRef](#)] [[PubMed](#)]
53. Piñero, J.; Saüch, J.; Sanz, F.; Furlong, L.I. The DisGeNET cytoscape app: Exploring and visualizing disease genomics data. *Comput. Struct. Biotechnol. J.* **2021**, *19*, 2960–2967. [[CrossRef](#)] [[PubMed](#)]
54. Wang, Y.; Zhang, S.; Li, F.; Zhou, Y.; Zhang, Y.; Wang, Z.; Zhang, R.; Zhu, J.; Ren, Y.; Tan, Y.; et al. Therapeutic target database 2020: Enriched resource for facilitating research and early development of targeted therapeutics. *Nucleic Acids Res.* **2020**, *48*, D1031–D1041. [[CrossRef](#)] [[PubMed](#)]
55. Shannon, P.; Markiel, A.; Ozier, O.; Baliga, N.S.; Wang, J.T.; Ramage, D.; Amin, N.; Schwikowski, B.; Ideker, T. Cytoscape: A software environment for integrated models of biomolecular interaction networks. *Genome Res.* **2003**, *13*, 2498–2504. [[CrossRef](#)] [[PubMed](#)]
56. Sherman, B.T.; Hao, M.; Qiu, J.; Jiao, X.; Baseler, M.W.; Lane, H.C.; Imamichi, T.; Chang, W. DAVID: A web server for functional enrichment analysis and functional annotation of gene lists (2021 update). *Nucleic Acids Res.* **2022**, *50*, W216–W221. [[CrossRef](#)]
57. Kanehisa, M.; Goto, S. KEGG: Kyoto encyclopedia of genes and genomes. *Nucleic Acids Res.* **2000**, *28*, 27–30. [[CrossRef](#)]

58. Szklarczyk, D.; Gable, A.L.; Nastou, K.C.; Lyon, D.; Kirsch, R.; Pyysalo, S.; Doncheva, N.T.; Legeay, M.; Fang, T.; Bork, P.; et al. The STRING database in 2021: Customizable protein-protein networks, and functional characterization of user-uploaded gene/measurement sets. *Nucleic Acids Res.* **2021**, *49*, D605–D612. [[CrossRef](#)]
59. Berman, H.M.; Westbrook, J.; Feng, Z.; Gilliland, G.; Bhat, T.N.; Weissig, H.; Shindyalov, I.N.; Bourne, P.E. The Protein Data Bank. *Nucleic Acids Res.* **2000**, *28*, 235–242. [[CrossRef](#)]
60. Trott, O.; Olson, A.J. AutoDock Vina: Improving the speed and accuracy of docking with a new scoring function, efficient optimization, and multithreading. *J. Comput. Chem.* **2010**, *31*, 455–461. [[CrossRef](#)]